



**HAL**  
open science

**Multiple widespread landslides during the long-term evolution of a volcanic island: Insights from high-resolution seismic data, Montserrat, Lesser Antilles**

E. Lebas, A. Le Friant, G. Boudon, S F L Watt, P. J. Talling, N. Feuillet, C. Deplus, C. Berndt, M E Vardy

► **To cite this version:**

E. Lebas, A. Le Friant, G. Boudon, S F L Watt, P. J. Talling, et al.. Multiple widespread landslides during the long-term evolution of a volcanic island: Insights from high-resolution seismic data, Montserrat, Lesser Antilles. *Geochemistry, Geophysics, Geosystems*, 2011, 12 (5), pp.Q05006. 10.1029/2010GC003451 . insu-01609924

**HAL Id: insu-01609924**

**<https://insu.hal.science/insu-01609924>**

Submitted on 4 Oct 2017

**HAL** is a multi-disciplinary open access archive for the deposit and dissemination of scientific research documents, whether they are published or not. The documents may come from teaching and research institutions in France or abroad, or from public or private research centers.

L'archive ouverte pluridisciplinaire **HAL**, est destinée au dépôt et à la diffusion de documents scientifiques de niveau recherche, publiés ou non, émanant des établissements d'enseignement et de recherche français ou étrangers, des laboratoires publics ou privés.



# Multiple widespread landslides during the long-term evolution of a volcanic island: Insights from high-resolution seismic data, Montserrat, Lesser Antilles

**E. Lebas, A. Le Friant, and G. Boudon**

*Institut de Physique du Globe de Paris, Sorbonne Paris Cité and CNRS UMR 7154, 1 rue Jussieu, F-75238 Paris CEDEX 05, France (lebas@ipgp.fr)*

**S. F. L. Watt**

*School of Ocean and Earth Science, University of Southampton, European Way, Southampton SO14 3ZH, UK*

**P. J. Talling**

*National Oceanography Centre Southampton, European Way, Southampton SO14 3ZH, UK*

**N. Feuillet and C. Deplus**

*Institut de Physique du Globe de Paris, Sorbonne Paris Cité and CNRS UMR 7154, 1 rue Jussieu, F-75238 Paris CEDEX 05, France*

**C. Berndt**

*Leibniz-Institute for Marine Sciences (IFM-GEOMAR), Wischhofstrasse 1-3, D-24148 Kiel, Germany*

*Also at National Oceanography Centre Southampton, European Way, Southampton SO14 3ZH, UK*

**M. E. Vardy**

*School of Ocean and Earth Science, University of Southampton, European Way, Southampton SO14 3ZH, UK*

[1] New high-resolution multichannel seismic data (GWADASEIS-2009 and JC45/46-2010 cruises; 72 and 60 channels, respectively) combined with previous data (AGUADOMAR-1999 and CARAVAL-2002; 6 and 24 channels, respectively) allow a detailed investigation of mass-wasting processes around the volcanic island of Montserrat in the Lesser Antilles. Seven submarine deposits have sources on the flanks of Montserrat, while three are related to the nearby Kahouanne submarine volcanoes. The most voluminous deposit ( $\sim 20 \text{ km}^3$ ) within the Bouillante-Montserrat half-graben has not been described previously and is probably related to a flank instability of the Centre Hills Volcano on Montserrat, while other events are related to the younger South Soufrière Hills-Soufrière Hills volcanic complex. All deposits are located to the south or southeast of the island in an area delimited by faults of the Bouillante-Montserrat half-graben. They cover a large part of the southeast quarter of the surrounding seafloor ( $\sim 520 \text{ km}^2$ ), with a total volume of  $\sim 40 \text{ km}^3$ . Our observations suggest that the Bouillante-Montserrat half-graben exerts a control on the extent and propagation of the most voluminous deposits. We propose an interpretation for mass-wasting processes around Montserrat similar to what has happened for the southern islands of the Lesser Antilles.

**Components:** 10,200 words, 9 figures, 2 tables.

**Keywords:** debris avalanches; flank collapse; submarine slope failure; Montserrat; Lesser Antilles.

**Index Terms:** 3070 Marine Geology and Geophysics: Submarine landslides; 3045 Marine Geology and Geophysics: Seafloor morphology, geology, and geophysics; 8404 Volcanology: Volcanoclastic deposits.

**Received** 2 December 2010; **Revised** 23 February 2011; **Accepted** 29 March 2011; **Published** 12 May 2011.

Lebas, E., A. Le Friant, G. Boudon, S. F. L. Watt, P. J. Talling, N. Feuillet, C. Deplus, C. Berndt, and M. E. Vardy (2011), Multiple widespread landslides during the long-term evolution of a volcanic island: Insights from high-resolution seismic data, Montserrat, Lesser Antilles, *Geochem. Geophys. Geosyst.*, 12, Q05006, doi:10.1029/2010GC003451.

## 1. Introduction

[2] Volcanic and tectonic processes on the flanks of oceanic islands considerably modify background marine erosion and sedimentation processes. Volcano flank instabilities have been recognized as recurrent processes [Siebert, 1984; McGuire, 1996] in oceanic intraplate islands such as Hawaii [Moore et al., 1989], the Canary Islands [Carracedo, 1999; Carracedo et al., 1999; Masson et al., 2002], La Réunion [Labazuy, 1996; Oehler et al., 2004, 2008], Tahiti [Clément et al., 2003], and in subduction zone settings such as the Lesser Antilles (47 events identified [Boudon et al., 2007]). Flank instabilities can affect either the subaerial or the submarine parts of volcanoes or both. Large flank failures typically lead to the formation of horseshoe scarp structures. The resulting debris avalanches may generate catastrophic tsunamis upon entering the sea and flowing along the seafloor [Camus and Vincent, 1983; Le Friant et al., 2003b, 2006; Tinti et al., 2006]. The triggering of flank instabilities can be related to volcanic or tectonic activity [McGuire, 1996; Voight and Elsworth, 1997; Ui et al., 2000; Voight, 2000]. The flow of debris avalanches is strongly influenced by surrounding topography. The abrupt entrance of huge volumes of material into the sea (more than 5000 km<sup>3</sup> in the Hawaiian Ridge [Moore et al., 1989]) results in large and complex submarine mass movements, which may erode the substratum [Gee et al., 2005; Bull et al., 2009] and drastically and rapidly alter sedimentation processes in the region [Schneider et al., 1997; Le Friant et al., 2003a; Dufresne et al., 2010].

[3] The island of Montserrat, located in the north of the Lesser Antilles Arc (Figure 1), has undergone multiple lava dome collapse events during the ongoing eruption (1995 to present). Previous work shows that the main part of material produced by the present eruption has been deposited underwater [Hart et al., 2004; Le Friant et al., 2004, 2009, 2010;

Trofimovs et al., 2006, 2008; Wadge et al., 2010]. Older and much larger submarine debris avalanche deposits there have been partially described by Le Friant et al. [2004], but the limited resolution and coverage of the data available then did not allow a complete view of the seafloor and subseafloor morphology around Montserrat. New high-resolution seismic data have been collected recently (GWADASEIS cruise 2009, 72 channels; JC45/46 cruise 2010, 60 channels) to investigate in detail the surrounding environment of Montserrat and to understand mass-wasting processes around the island. These data complement other data previously acquired (AGUADOMAR cruise 1999, 6 channels; CARVAL cruise 2002, 24 channels), and the combined Montserrat data set is now the most complete of any Lesser Antilles volcano. The combined data are important for understanding tectonic and sedimentary processes around a volcanic island in an oceanic context. These data may be used to address such questions as: How does the formation of a volcanic island influence local sedimentation processes? What is the range of mass-wasting processes around the island? Can we quantify the proportion and distribution of volcanic material that enters the sea? What is the link between tectonic structures and volcanic instabilities and dispersal of mass movement products?

[4] In this paper, we study the mass-wasting processes around Montserrat (Lesser Antilles) using the complete marine geophysical data set collected during the four oceanographic cruises mentioned above. We first redefine the lateral extents of previously identified deposits [e.g., Le Friant et al., 2004] and then highlight major new deposits discovered within the Bouillante–Montserrat half-graben and near the Kahouanne Volcanoes. We then discuss the characteristic features, the volumes, the origins and the distribution of submarine deposits identified around the island. Last, we propose an interpretation for mass-wasting processes around

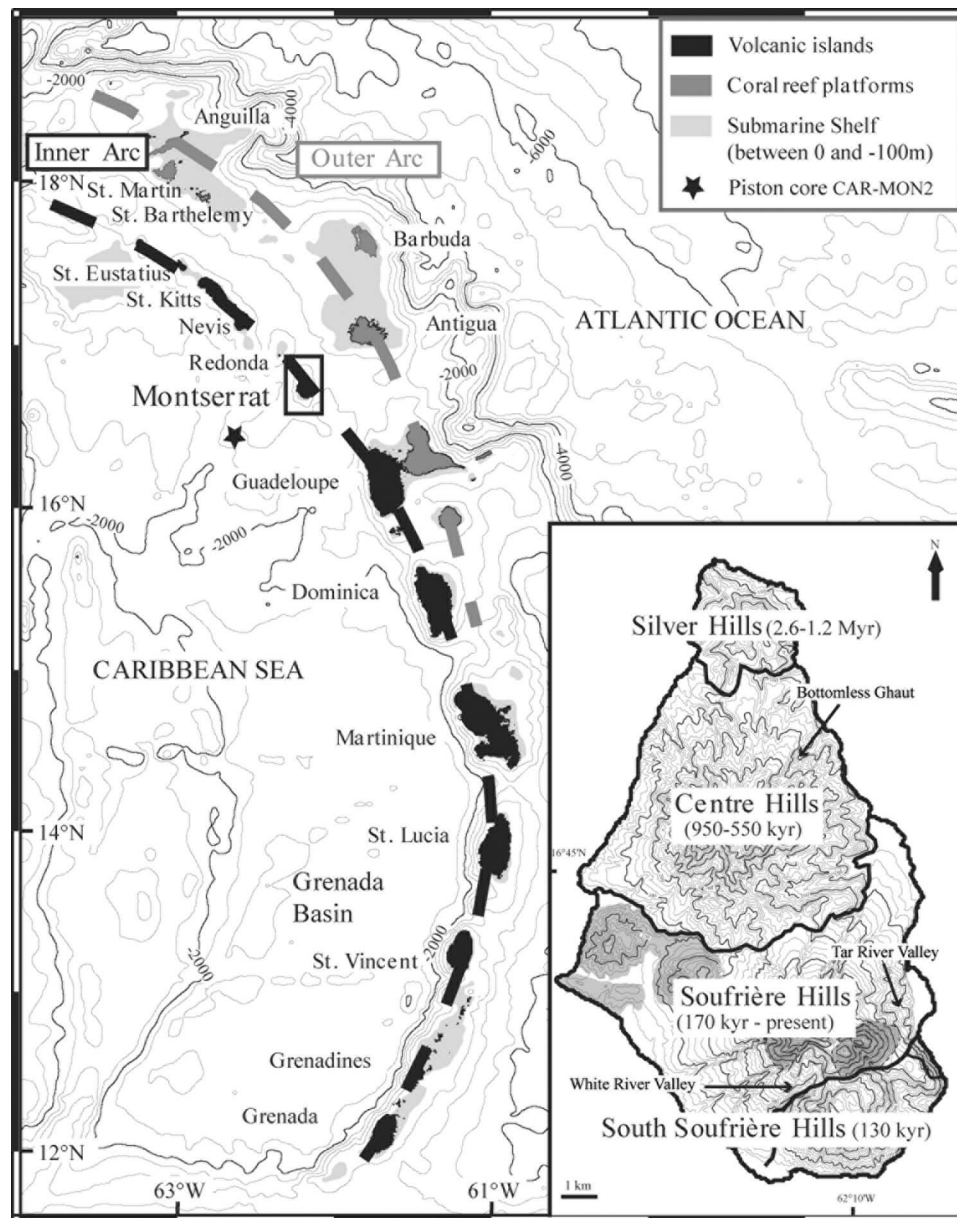


**Figure 1.** Geodynamic setting of the Lesser Antilles Arc. Predicted bathymetry from *Smith and Sandwell* [1997]. Contour interval is 500 m with 2000 m contour in bold. The volcanic islands (inner arc) are in dark and the coral reef platforms (outer arc) are in dark gray. Star represents the location of the piston core (CAR-MON2) collected during the CARAVAL cruise in 2002 (16°27.699'N, 62°38.077'W). Inset: topographic map of Montserrat from the 10 m DEM (contour interval: 25 m) showing the four volcanic edifices and the volcanism evolution from north to south. The digital elevation model (DEM) has been provided by G. Wadge. The ages are from *Harford et al.* [2002].

Montserrat by considering the influence of the Bouillante-Montserrat half-graben and by comparing Montserrat with the southern islands of the Lesser Antilles Arc.

## 2. Data Collection and Analysis

[5] This paper is based on marine geophysical data collected during four oceanographic cruises, as

mentioned previously (Figure 2). Swath bathymetry and backscatter data were collected using the Simrad EM12D system during the AGUADOMAR (1999) and CARAVAL (2002) cruises, the Simrad EM300 system during the GWADASEIS (2009) cruise, and the Simrad EM120 system during the JC45/46 (2010) cruise. Swath data presented here were processed using the CARAIBES software developed by Ifremer. Digital terrain models were constructed

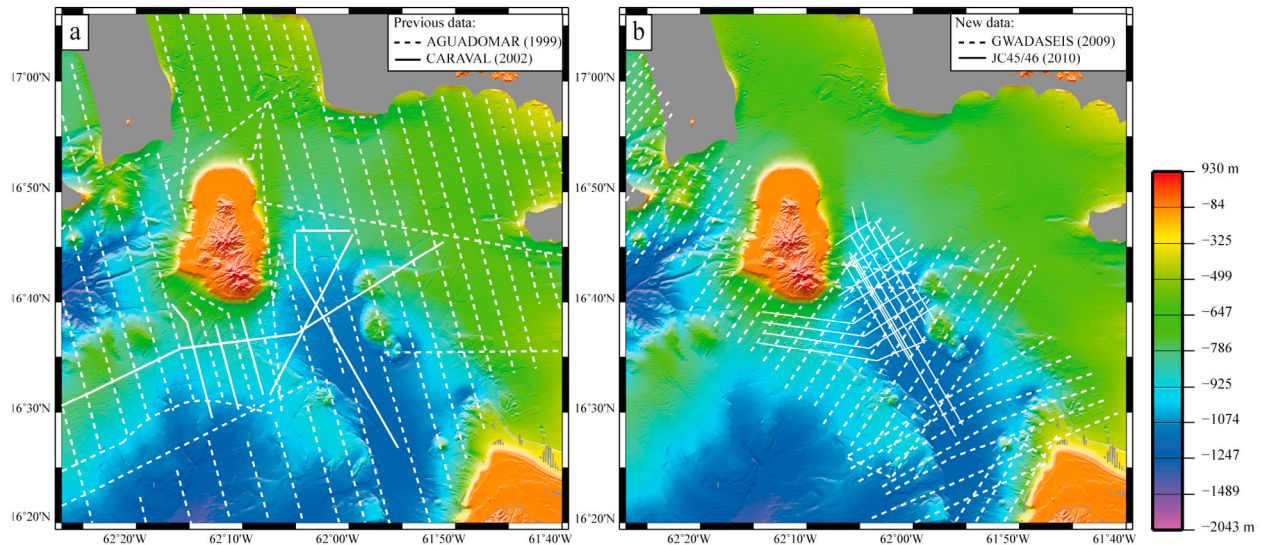


**Figure 2.** Topography and bathymetry of Montserrat illuminated from NNW. The bathymetry results from the combination of the AGUADOMAR (1999) and GWADASEIS (2009) data. Color scale is relative to sea level. (a) Previous data: location of seismic reflection profiles collected during the AGUADOMAR cruise in dashed lines (1999; 6 channels) and during the CARAVAL cruise in solid lines (2002; 24 channels). (b) New data: location of high-resolution seismic reflection profiles collected during the GWADASEIS cruise in dashed lines (2009; 72 channels) and during the JC45/46 cruise in solid lines (2010; 60 channels).

with resolutions of 100 m, 50 m or 25 m according to the depth of the seafloor surrounding the island. In addition, we collected 3.5 kHz echo sounder profiles during the AGUADOMAR and CARAVAL cruises and chirp subbottom profiles during the GWADASEIS and JC45/46 cruises.

[6] Seismic reflection profiles were collected around the island using three different systems (Figure 2 and Table 1). Six-channel seismic reflection profiles were collected up to 75 km from the coastline in 1999. Seismic profiles with higher resolution were collected using a 24-channel streamer in 2002, with streamer and air guns towed closer to the sea surface. High-resolution seismic reflection profiles were acquired in 2009 (72 channels) and 2010 (60 channels). Navigation used Starfix differential global positioning system (GPS) during the AGUADOMAR cruise and GPS with no degradation during the CARAVAL, GWADASEIS and JC45/46 cruises.

A positioning accuracy of a few meters was achieved. The multichannel seismic reflection data were filtered, stacked and migrated using the Seismic Unix software [Cohen and Stockwell, 1996] for the 1999, 2002 and 2009 data, and with Landmark's ProMAX© software for the 2010 data. The AGUADOMAR and CARAVAL data were migrated at a seawater velocity of  $1450 \text{ m s}^{-1}$ , a NMO correction was applied for the GWADASEIS data, and the JC45/46 data were migrated at a linearly increasing velocity of  $1490\text{--}2500 \text{ m s}^{-1}$ . The vertical resolutions of the new seismic data are about 3 m and 4 m (GWADASEIS and JC45/46, respectively) while the resolutions of the earlier data were only around  $\sim 10$  to  $\sim 20$  m.

[7] All the processed data have been combined and analyzed using Kingdom Suite© software, which allows correlation of reflectors between different lines and distinction of superimposed chaotic units.

**Table 1.** Summary of Acquisition Parameters for Seismic Data Used<sup>a</sup>

Oceanographic Cruise	Sources (cu in.)	Number of Guns	Gun Depth (m)	Number of Recording Channels	Channel Spacing (m)	Streamer Depth (m)	Streamer Length (m)	Vertical Resolution (m)
AGUADOMAR (1999)	GI 45/45 and 105/105	2	7	6	50	5	530	$\sim 20$
CARAVAL (2002)	GI 45/45	2	1.5	24	12.5	3	$\sim 500$	$\sim 10$
GWADASEIS (2009)	GI 35/35 and 45/45	4	3	72	6.25	3	358	3
JC45/46 (2010)	GI 105/45	2	3	60	1	1	100	4

<sup>a</sup>GI Air gun volumes given as generator volume/injector volume in cubic inches.

**Table 2.** Characteristics and Source Locations of the Debris Avalanche Deposits Identified Offshore Montserrat and Near the Kahouanne Volcanoes<sup>a</sup>

Deposit	Depth	Direction	Event	Run Out <sup>b</sup> (km)	Extent (km <sup>2</sup> )	Mean Thickness (s twt)	Average Thickness (m)					Volume (km <sup>3</sup> )		
							2000 m s <sup>-1</sup>	2150 m s <sup>-1</sup>	2200 m s <sup>-1</sup>	2000 m s <sup>-1</sup>	2150 m s <sup>-1</sup>	2200 m s <sup>-1</sup>	2000 m s <sup>-1</sup>	2150 m s <sup>-1</sup>
1	Sf	East-Southeast	English's Crater + another event	12	51	0.046	46	49	51	1.7	1.8	1.8	1.8	
2	Sb	Southeast	Submarine slope failure C2	30	190	0.058	58	62	64	8.4	9	9.2	9.2	
3	Sf	South	Submarine slope failure C3?	11.7	59	0.027	27	29	30	1.2	1.3	1.3	1.3	
4	Sb	South-Southwest?	Submarine? On-land?	9	69	0.038	38	41	42	3.2	3.4	3.5	3.5	
5	Sf	Southwest	Submarine slope failure C4	9	27	-	-	-	-	-	~0.3 <sup>c</sup>	-	-	
8	Db	Southeast	Centre Hills Volcano	31	277	0.087	87	94	96	18.6	~20	20.5	20.5	
9	Db	East	Centre Hills Volcano	14.7	23	0.039	39	42	43	0.8	~0.9	0.9	0.9	
10	Db	North-Northeast	Seamount B, Kahouanne Volcanoes	~5	61	0.103	103	111	113	4.0	4.3	4.4	4.4	
11	Db	Southwest?	?	up to 2.5	~10	0.036	36	39	40	0.4	~0.4	0.4	0.4	
12	Sb	Southwest	Seamount A, Kahouanne Volcanoes	2.1	~5.5	0.037	37	40	41	0.2	~0.2	0.2	0.2	

<sup>a</sup>Deposits thicknesses are obtained using the seismic velocity of 2150 m s<sup>-1</sup> deduced from the JC45/46 data analysis. Different seismic velocities commonly used in literature for similar deposits (2000 m s<sup>-1</sup> [Bull et al., 2009]; 2200 m s<sup>-1</sup> [Feuillet et al., 2010; Paulatto et al., 2010]) give a range of uncertainties linked to velocity choice. The volumes are estimated using those different seismic velocities and Kingdom Suite© software allows accurate volume estimations, taking into account lateral thickness variations of the deposits. Sf, Sb, and Db refer to the depth location of deposits (surficial, shallowly buried, and deeply buried, respectively).

<sup>b</sup>Given from the coastline.

<sup>c</sup>Volume estimated using a mean deposit thickness of 10 m [Le Friant et al., 2004].

To estimate the average thickness of intervening units, we selected as our best value the seismic velocity of 2150 m s<sup>-1</sup>, derived from JC45/46 seismic data analysis (common reflection point NMO velocity picking). This value is slightly higher than some assumed velocity used previously in similar deposits (e.g., 1800 m s<sup>-1</sup> [Urgeles et al., 1997; Collot et al., 2001; Le Friant et al., 2004], 2000 m s<sup>-1</sup> [Bull et al., 2009]) but close to 2200 m s<sup>-1</sup> used recently [Feuillet et al., 2010; Paulatto et al., 2010]. To have an order of magnitude of uncertainties on thickness deposits, we have considered the assumption of a range of seismic velocities, from 2000 m s<sup>-1</sup> to 2200 m s<sup>-1</sup> (Table 2). Volumes of intervening units have been calculated using the same average seismic velocity of 2150 m s<sup>-1</sup> and using the Kingdom Suite© software which takes into account lateral thickness variations along the profile. To consider uncertainties related to the seismic velocity used, a range of volumes is given using the minimum and maximum values of seismic velocities (Table 2).

### 3. Geological Setting and Regional-Scale Bathymetry

#### 3.1. The Lesser Antilles Arc

[8] Montserrat belongs to the Lesser Antilles Arc, which results from subduction of the Atlantic oceanic lithosphere under the Caribbean Plate at a rate of ~2 cm/yr [Wadge, 1984; DeMets et al., 2000] (Figure 1). Arc volcanism has occurred since 40 Myr [Martin-Kaye, 1969; Bouysse et al., 1990]. The northern part of the arc is divided into two chains of islands: the outer (eastern) chain corresponds to an older, inactive arc where thick carbonate platforms cover a volcanic basement, whereas the inner (western) arc has been active since 20 Myr and contains all of the presently active volcanoes [Bouysse et al., 1990]. Montserrat belongs to the northern part of the inner arc. To the south, the arc is composed of only one chain of islands on which the older and recent parts are superimposed. These southern islands are bordered to the west by the back-arc Grenada Basin, which is up to 2.9 km deep.

[9] The subaerial volcanic activity on Montserrat covers a period from 2.6 Myr to present, and the active volcanic centers have generally migrated from north to south [Harford et al., 2002] (Figure 1). The three main volcanic centers are Silver Hills (~2.6 Myr to 1.2 Myr), Centre Hills (at least ~950 to ~550 kyr) and South Soufrière Hills (~130 kyr)–

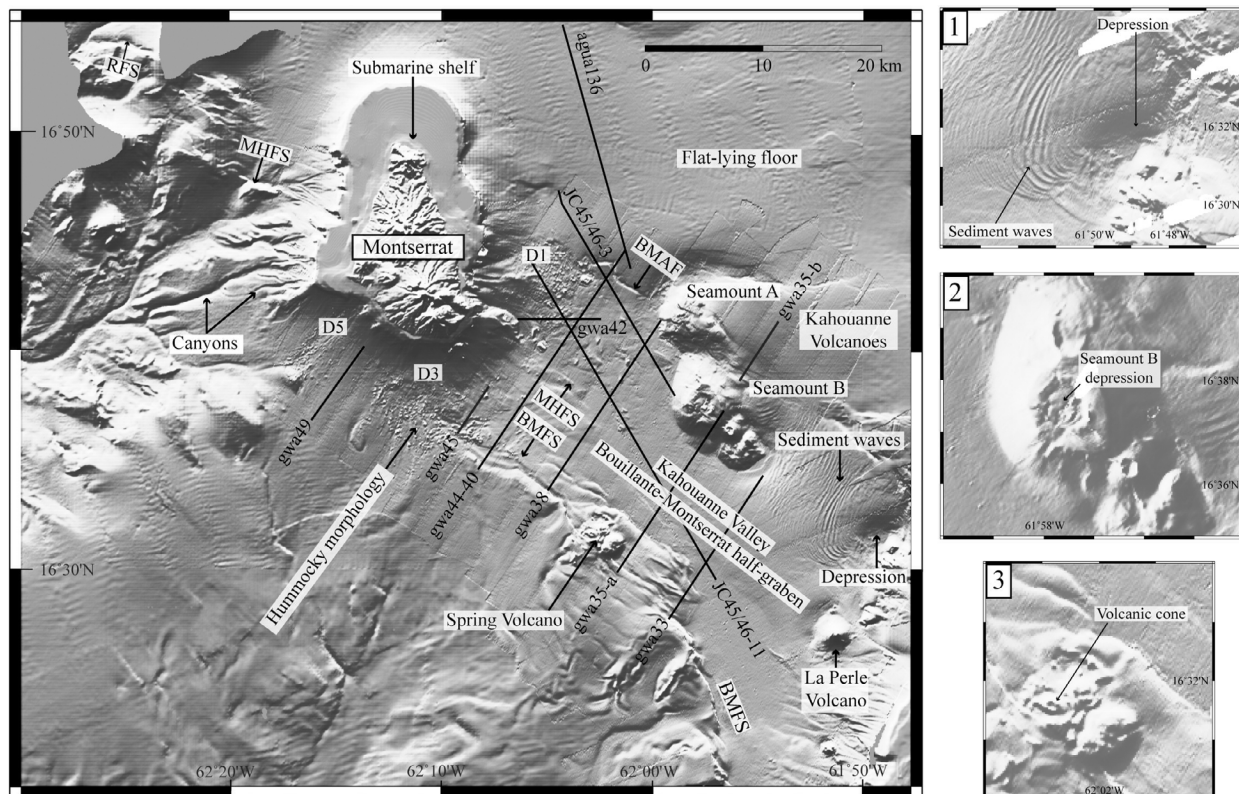


**Figure 3.** Shaded image of the topography and bathymetry of Montserrat illuminated from NNW. Key morphological features identified offshore Montserrat and within the Bouillante-Montserrat half-graben are labeled. D1, D3, and D5 correspond to debris avalanche deposits, and MHFS, BMFS, and BMAF correspond to the major fault systems documented by *Feuillet et al.* [2010]. Solid lines represent the seismic profiles shown in Figures 4, 5, and 6. Insets: shaded images of bathymetry showing in detail the sediment waves recognized southeast of the Kahouanne Volcanoes (1), the morphological features identified on seamount B (2), and the Spring Volcano (3).

Soufrière Hills (at least ~170 kyr to present) [*Harford et al.*, 2002].

### 3.2. Seafloor Morphology Around Montserrat

[10] The morphological features of the seafloor around Montserrat (from the coastline toward the open sea) are briefly summarized based on previous work [*Deplus et al.*, 2001; *Le Friant et al.*, 2004; *Feuillet et al.*, 2010] (Figure 3).

[11] The island is bordered by a shallow submarine shelf of variable width (maximum 5 km around Silver Hills) that extends to a maximum water depth of ~100 m. This shelf was formed from erosion during repeated glacioeustatic sea level fluctuations [*Le Friant et al.*, 2004].

[12] The steeper submarine flanks of the island extend down to water depths of 750–1000 m. Numerous canyons form tributaries to a large undersea valley west of the island (Figure 3), while

deep canyons do not occur on the other submarine flanks of Montserrat. The area north of Montserrat beyond the latitude of the Silver Hills displays a particularly contrasting flat-lying seafloor. Three areas of rough, blocky topography on the southeastern and southern submarine flanks of the island, reported by *Deplus et al.* [2001], correspond to the debris avalanche deposits 1, 3 and 5 described by *Le Friant et al.* [2004]. Similar blocky debris avalanche deposits have been observed on the submarine flanks of neighboring islands Redonda and Antigua [*Le Friant et al.*, 2004] (Figure 1). Submarine flow deposits associated with recent (1996–present) dome collapses of Soufrière Hills Volcano occur closer to the island, especially offshore from the Tar River Valley. These deposits were formed by pyroclastic flows that traveled down either the Tar River or White River valleys before entering the sea. Descriptions of these events and their deposits are provided by *Cole et al.* [2002], *Sparks et al.* [2002], *Hart et al.* [2004], *Herd et al.* [2005], *Trofimovs et al.* [2006, 2008], and *Le Friant et al.* [2009, 2010].

[13] Three major fault systems have been identified by *Feuillet et al.* [2010] and new observations have been added by *Kenedi et al.* [2010] during the SEA-CALIPSO cruise: the Montserrat-Havers Fault System (MHFS) and Redonda Fault System (RFS) northwest of Montserrat, and the Bouillante-Montserrat Fault System (BMFS) southeast of Montserrat. The MHFS continues across the island, and is interpreted to extend offshore to the southeast (Figure 3). The BMFS dominantly dips northeast and is composed of 10 to 20 km long normal fault segments, with a strike of  $\sim 130$  deg ( $\pm 20$  deg), arranged in a right-stepping en echelon pattern that extends to Basse-Terre on Guadeloupe. The BMFS delimits the western side of the Kahouanne Valley (10 to 17 km wide, and  $\sim 50$  km in length), which is a typical half-graben (e.g., Bouillante-Montserrat half-graben; Figure 3). Three submarine volcanic edifices have been identified within or at the edges of the Kahouanne Valley: the Kahouanne, Spring and La Perle volcanoes. The Kahouanne Volcanoes (seamounts A and B; Figure 3) are located roughly east-southeast of Montserrat ( $\sim 22$  km from the coastline for the seamount B). They are crosscut and left-laterally displaced by  $\sim 4$  km from each other by the large-scale transtensional Bouillante-Montserrat Fault System [*Feuillet et al.*, 2010].

### 3.3. New Observations From 2009 High-Resolution Bathymetry

[14] New high-resolution bathymetric data collected in 2009 allow us to describe the morphological characteristics of the Kahouanne Volcanoes in more detail (Figure 3). Seamount A has an elongated shape with dimensions of  $\sim 5$  by  $\sim 3$  km, and rises to a height of at least 665 m above the graben floor. Its flat summit displays several scarps. Seamount B has dimensions of  $\sim 5.0$  km by 5.3 km, and a height of at least 823 m above the graben floor. A northwest-southeast orientated depression (1.5 by 1.6 km) occurs on seamount B, which also has a fault crossing its flat summit. A smaller volcanic cone southeast of seamount B displays a crater on its summit with a diameter of  $\sim 550$  m. The flattened summits of both seamounts A and B would suggest relatively old ages for the volcanic activity. The Spring Volcano ( $\sim 1.5$  by  $\sim 1.2$  km) is located on the west side of the Kahouanne Valley above the BMFS. A volcanic cone with a  $\sim 250$  m wide summit crater occurs  $\sim 1$  km northwest of the Spring Volcano and is probably associated to it. La Perle Volcano is located  $\sim 19$  km southeast of the Spring Volcano, and comprises a km diameter cone that is  $\sim 800$  m in height. A horseshoe-shaped structure open to the south

( $\sim 855$  m width) is observed on its southern flank, in which a subsequent cone has grown. The relatively smooth form of La Perle Volcano, without extensive fault or erosional scarps and the absence of sedimentary layers on 3.5 kHz data, suggest a relatively young age.

[15] The new high-resolution bathymetry survey also shows a previously unknown but well developed field of sediment waves to the southeast of the Kahouanne Volcanoes (Figure 3). The sediment waves are located downslope from an ENE-WSW elongated depression (1.7 by 3.4 km) within the Kahouanne Valley, and the sediment wavefield covers an area of  $\sim 50$  km<sup>2</sup>. The waves are roughly orientated NE-SW and comprise two sets. The first set of waves is located close to the depression, and has larger wavelengths and wave heights ( $\sim 340$  m; up to 21 m, respectively). The second wavefield has smaller wavelengths of  $\sim 115$  m ( $\sim 1/3$  of the first set) and heights up to  $\sim 8$  m. The maximum length of wave crests reaches  $\sim 8$  km and is observed within the first set.

## 4. Submarine Landslide Deposits Offshore Montserrat

[16] The high-resolution seismic reflection data collected during 2009 and 2010 provide new information on the number, extent, shape and internal character of submarine landslide deposits around Montserrat.

[17] The extent of deposits is deduced from a combined analysis of swath bathymetry, 3.5 kHz profiles and seismic reflection data. On seismic profiles, debris avalanche deposits display typical chaotic reflectors which differ from well-bedded sedimentary units (Figure 4). The high vertical resolution of the new data (GWADASEIS, JC45/46; Table 1) has allowed us to clearly distinguish superimposed landslide deposits at depth by highlighting well-bedded sedimentary units lying between landslide units (Figures 4b, 4c, 5a, 5b, 5c, and 6). The high resolution has also permitted us to accurately locate the upper and lower boundaries of each debris avalanche deposit, and to therefore estimate deposit thickness. Different subunits inside the deposits have also been recognized by the presence of irregular and discontinuous, strong reflectors (Figures 5b and 6).

[18] Some of the deposits recognized in this study were described previously by *Le Friant et al.* [2004]. We have retained the deposit numbering system

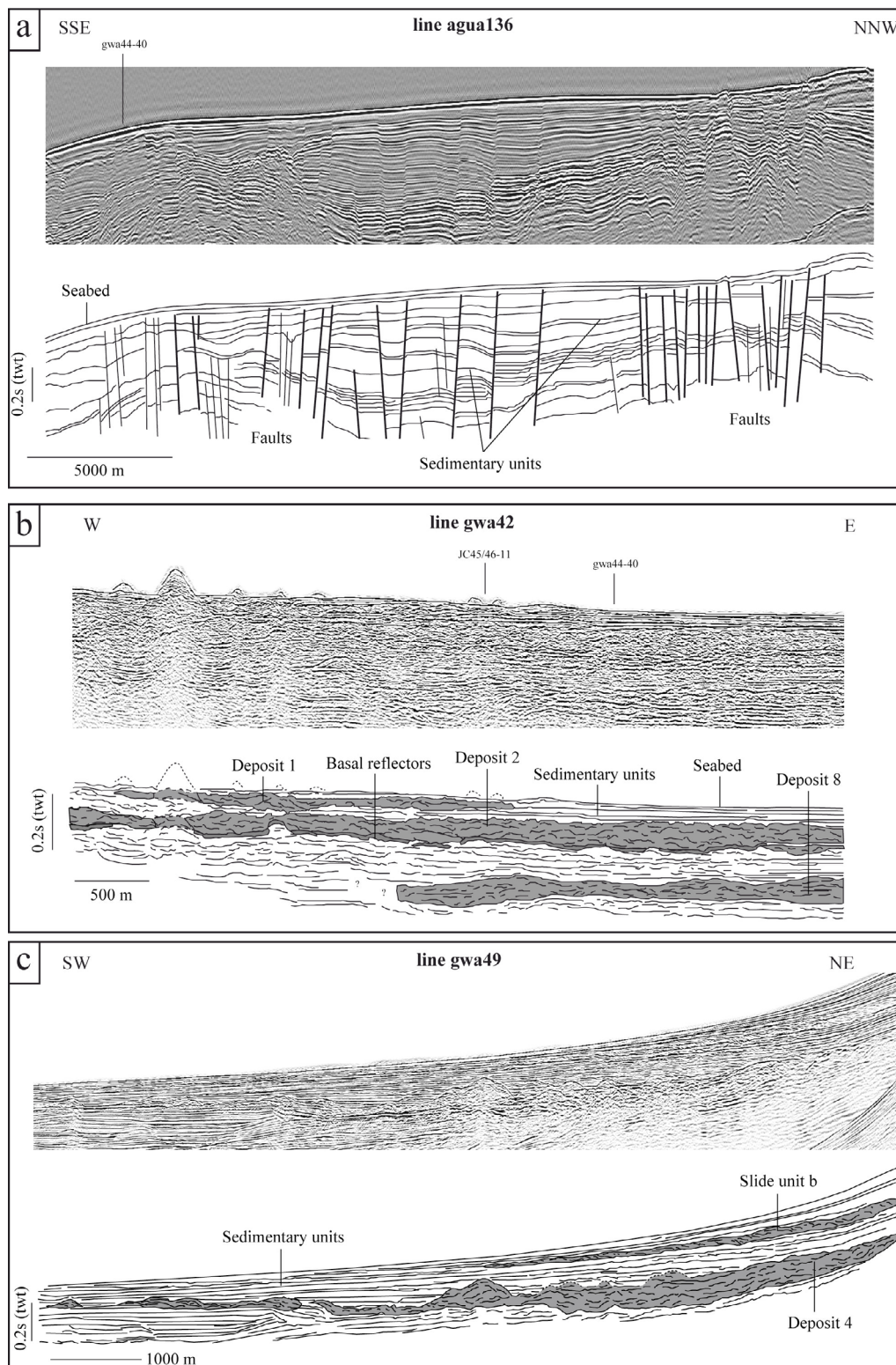


**Figure 4.** AGUADOMAR and GWADASEIS seismic reflection profiles revealing the presence of debris avalanche deposits offshore the southeast part of Montserrat only. Location of profiles is shown in Figure 3. Debris avalanche deposits (in gray in line drawings) are characterized by chaotic reflectors that contrast with well-bedded subhorizontal sedimentary units. Twt, two-way travel time. (a) Line agua136 shows the absence of debris avalanche deposits north of Montserrat. Sedimentary units are crosscut by numerous faults. (b) Line gwa42 crosses the deposits 1, 2, and 8, which are separated by sedimentary units. (c) Line gwa49 crosses the deposit 4.

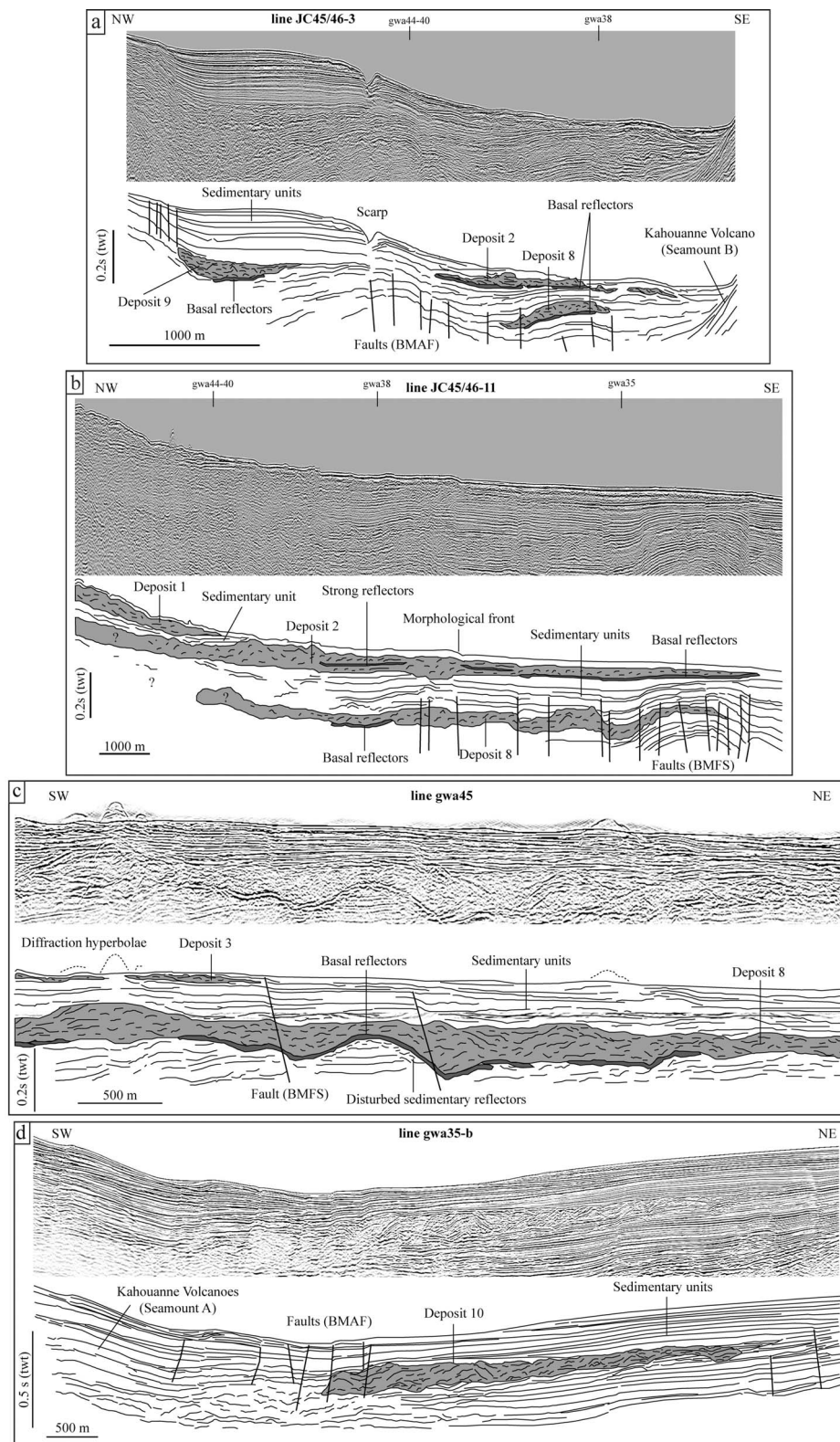


**Figure 5.** JC45/46 and GWADASEIS seismic reflection profiles underlying the presence of debris avalanche deposits offshore Montserrat. Location of profiles is shown in Figure 3. Twt, two-way travel time. (a) Line JC45/46-3 crosses the deposits 2, 8, and 9. (b) Line JC45/46-11 crosses the deposits 1, 2, and 8, which are separated by thick sedimentary units within the Bouillante-Montserrat half-graben. (c) Line gwa45 crosses the deposits 3 and 8 illustrating the undulated shape of the deposit 8 basal reflectors near the island. (d) Line gwa35-b crosses deposit 10.

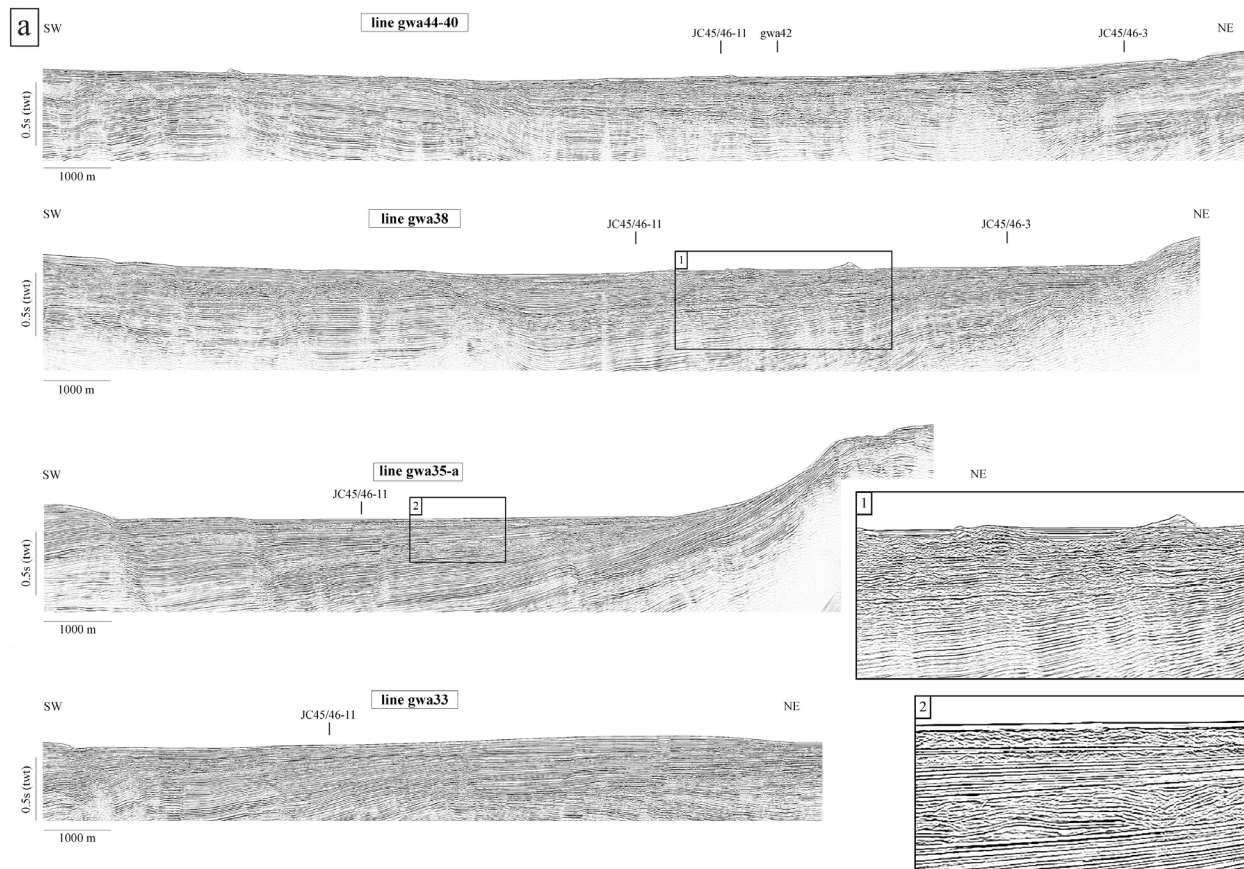


**Figure 6.** (a) GWADASEIS seismic reflection profiles showing the evolution of debris avalanche deposits within the Bouillante–Montserrat half-graben. (b) Interpreted sections of the GWADASEIS seismic profiles shown in Figure 6a. Location of profiles is shown in Figure 3. Twt, two-way travel time.

of this earlier study, extended with new numbers for the newly identified deposits (Figure 7). Some local small units visible only on one seismic profile have been referenced as slide units (slide units a and b; Figures 4c, 6 (line gwa44–40), and 7) since they could not be defined as extended deposits.

#### 4.1. The Eastern Submarine Flank of Montserrat and the Bouillante–Montserrat Half-Graben

[19] The new data enable us to improve the lateral extent and volume estimations for deposits 1 and 2 of *Le Friant et al.* [2004], and allow even larger and more deeply buried landslide deposits to be identified.

##### 4.1.1. Deposit 1

[20] Deposit 1 is located offshore from the Tar River Valley, and its base is clearly defined by an underlying well-bedded sedimentary unit (Figures 4b

and 5b). Deposit 1 typically has a hummocky facies seen in both bathymetric and seismic data (Figures 3 and 4b). The deposit spreads radially, with a width of up to 8.7 km (comparable to its downslope length of ~9 km) to cover an area of 51 km<sup>2</sup> that reaches ~12 km east-southeast from the coastline. It has a thickness of ~50 m and a volume of 1.8 km<sup>3</sup>, much larger than estimated previously by *Le Friant et al.* [2004], and extends further to the west and south with respect to its earlier mapping (Figure 7).

##### 4.1.2. Deposit 2

[21] Deposit 2 is located below deposit 1 and was emplaced over well-bedded sediment layers (Figures 4b, 5a, 5b, and 6). It is separated from deposit 1 by sedimentary units that are ~35 m thick in average (Figures 4b and 5b). Deposit 2 is much larger than deposit 1 and extends for ~30 km from the coastline in a southeast direction, covering an area of 190 km<sup>2</sup> (Figure 7). Deposit 2 displays

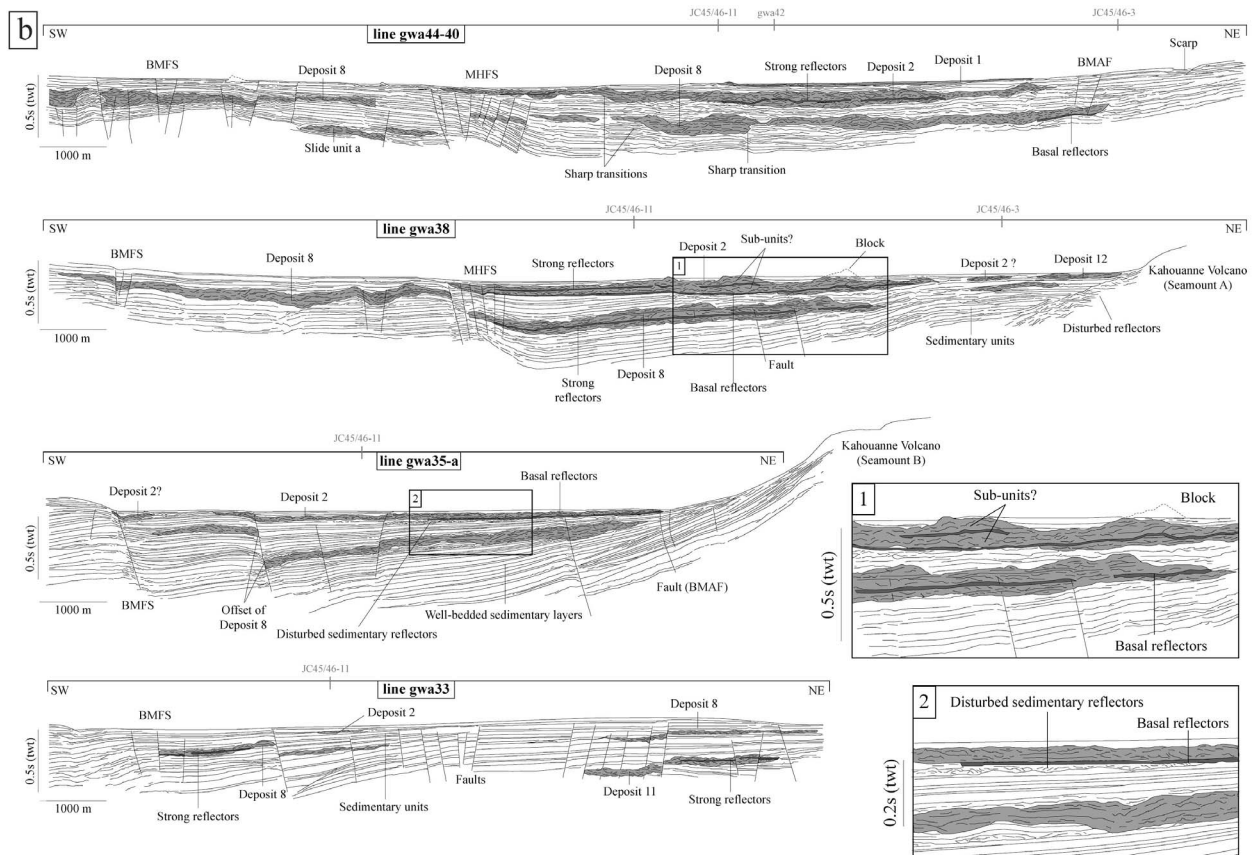


Figure 6. (continued)

important thickness variations, not previously identified, along each seismic profile. Thickness varies from ~100 m, and as much as ~135 m in local accumulation zones, to ~50 m on line gwa38 (Figure 6); the average is ~62 m. The deposit volume is estimated as ~9 km<sup>3</sup>. Strong, continuous flat reflectors are identified at the base of the chaotic unit that makes up deposit 2 (Figures 4b, 5a, 5b, and 6). Continuous reflectors are also sometimes clearly seen *within* deposit 2, such as on the line gwa38 (Figure 6). Below the strong basal reflectors there is a thin disturbed unit (~17 m thick in average up to 35 m on line gwa35-a; Figure 6, inset 2). The deposit is cut by faults of the MHFS close to the island and BMFS further offshore (Figures 3 and 6). The maximum offset observed, induced by faulting within deposit 2, occurs along the BMFS and is ~34 m (Figure 6, line gwa35-a).

#### 4.1.3. Deposit 8

[22] A newly identified mass flow deposit (deposit 8) represents the largest and deepest large-

scale chaotic unit imaged within the Bouillante-Montserrat half-graben. A smaller chaotic unit (deposit 11) has been identified below it (Figure 6, line gwa33). Deposit 8 is located underneath deposits 1, 2 and 3 and extends in a southeastern direction (Figures 5a, 5b, 5c, 6, and 7). The deposit comprises two chaotic lobes east and west of the MHFS (Figure 6, line gwa44-40). The two lobes occur at the same stratigraphic level once this fault offset is taken into account, and the two chaotic lobes were once continuous across the graben (Figure 7). Consequently, the two lobes constitute a single debris avalanche deposit, which is the largest yet identified off the island of Montserrat. Deposit 8 ran out for ~31 km from the coastline and covers an area of ~277 km<sup>2</sup> (Figure 7). The thickness of deposit 8 along the seismic profiles varies, e.g., from ~85 to ~115 m on line gwa38 (Figure 6), with an average of ~94 m. Its volume is estimated to be ~20 km<sup>3</sup>. Deposit 8 is separated from the overlying deposit 2 by ~100 m thick units of continuous reflectors in average. The base of deposit 8 is defined by strong reflectors, as was the case for deposit 2

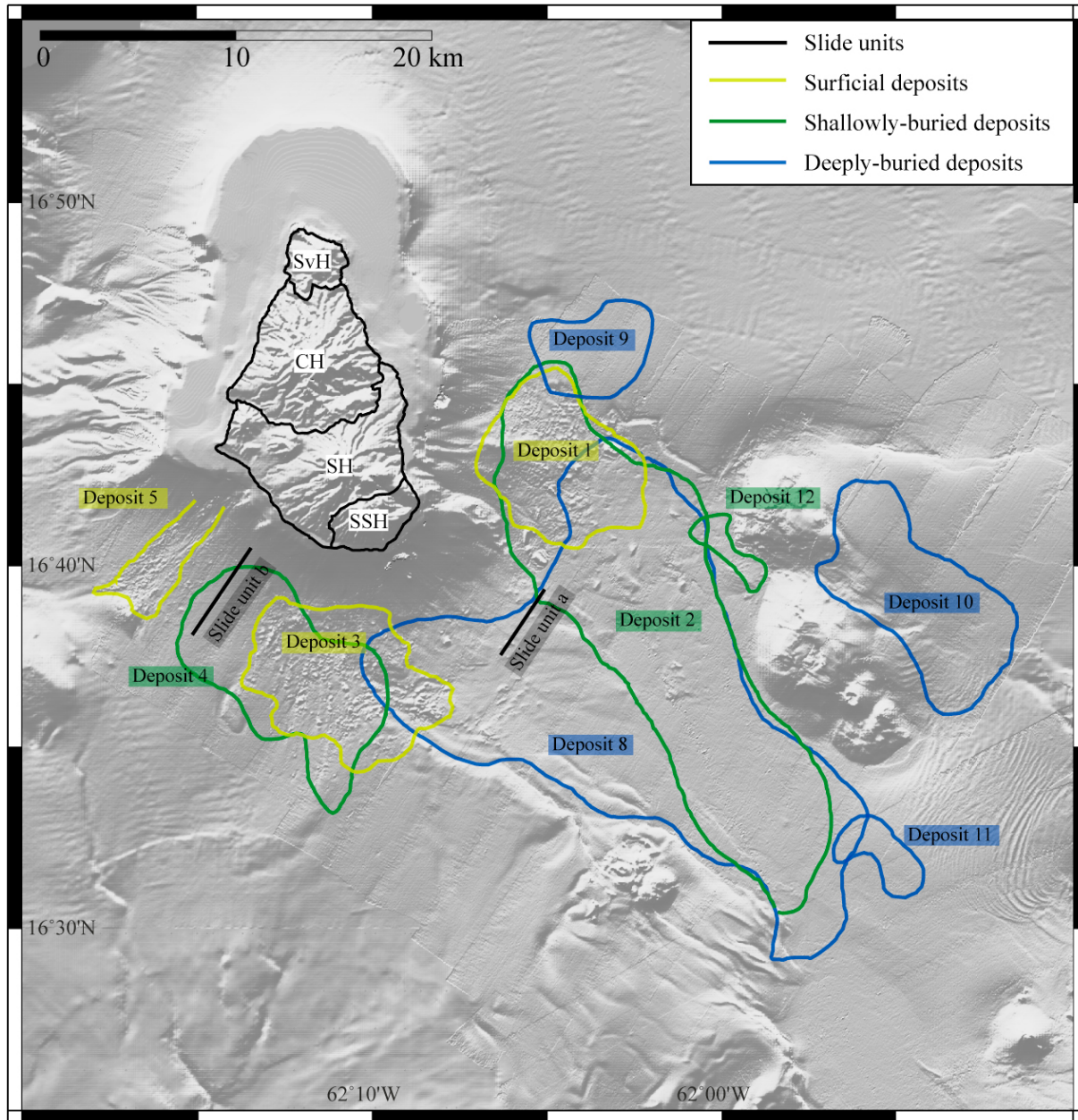


**Figure 7.** Shaded image of topography and bathymetry of Montserrat illuminated from NNW showing the importance of widespread mass-wasting events offshore. Light green lines show extents of surficial debris avalanche deposits with hummocky topography identified on bathymetry data. Dark green lines refer to shallowly buried deposits, and blue lines refer to deeply buried ones, both identified on seismic data. Landslides identified only on a single seismic line (i.e., slide units) are shown by black lines.

(Figures 5a, 5b, 5c, and 6). On seismic line gwa38, strong continuous reflectors also appear within the deposit (Figure 6). These internal reflectors display an undulating shape near the island (Figure 5c), whereas further offshore a flatter geometry is observed. Below deposit 8, a local chaotic unit (slide unit a) has been identified only on the seismic profile

gwa44–40 (Figure 6). This slide unit a is separated from deposit 8 by ~200 m of sedimentary units and covers ~4 km on the profile. The mean thickness of this slide unit is ~67 m. The three fault systems east and southeast of Montserrat (BMFS, MHFS, BMAF) crosscut deposit 8. The maximum offset of deposit 8 is induced by a major fault in the

Bouillante–Montserrat system (BMFS; southwest side) and this offset is estimated to be  $\sim 285$  m (Figure 6, line gwa35-a).

#### 4.1.4. Deposit 9

[23] Deposit 9 is located east of Montserrat offshore from the Centre Hills Volcano. It is covered by a thick ( $\sim 210$  m) sedimentary unit (Figure 5a). The deposit extends up to 14.7 km from the coastline in an eastward direction and covers an area of  $\sim 23$  km<sup>2</sup> (Figure 7). The maximum dimensions are 6.8 km (W-E) by 4 km (N-S). The average thickness of this chaotic unit is  $\sim 42$  m, resulting in an estimated volume of  $\sim 0.9$  km<sup>3</sup>.

## 4.2. The Southern and Southwestern Submarine Flanks of Montserrat

### 4.2.1. Deposits 3, 4, and 5

[24] The new seismic data further constrain the extents and volumes of deposits 3, 4 and 5 that were previously documented by *Le Friant et al.* [2004]. Deposit 5 is located on the southwestern submarine flank of Montserrat and has a hummocky morphology (Figure 3). It extends 9 km from the coastline toward the southwest, until it abuts a small submarine hill (Figure 7). The deposit covers an area of  $\sim 27$  km<sup>2</sup>, with a maximum width of  $\sim 3$  km in the distal part. The deposit volume is approximated at 0.3 km<sup>3</sup>, taking a mean thickness of  $\sim 10$  m (based on the height of blocks estimated by *Le Friant et al.* [2004]).

[25] Deposit 3 is located offshore from the White River Valley, south of Montserrat, and also displays a hummocky morphology (Figure 3). It extends for 11.7 km from the coastline in a southerly direction and covers an area of 59 km<sup>2</sup> (Figure 7). Its shape and hummocky character are comparable to that of deposit 1. The average thickness of deposit 3 is approximately 29 m and it has a volume of  $\sim 1.3$  km<sup>3</sup>. No resolvable sedimentary drape is observed above deposit 3 on the 3.5 kHz data [*Le Friant et al.*, 2004].

[26] Deposit 4 is located below deposit 3 (Figure 7). The two deposits are separated by sedimentary units that are  $\sim 30$ – $40$  m thick. Deposit 3 reaches 9 km from the coastline in a south-southwest direction and extends for 14 km in a south direction, covering an area of  $\sim 69$  km<sup>2</sup>. The mean thickness of deposit 4 decreases offshore from  $\sim 85$  m to 41 m (Figure 4c), and it has a volume of  $\sim 3.4$  km<sup>3</sup>. No strong coherent internal reflectors are observed within this chaotic unit but important thickness variations suggest the

occurrence of megablocks within deposit 4. Above deposit 4, a local thin slide unit b is identified (Figure 4c). It is separated from deposit 4 by sedimentary units that are  $\sim 110$  m thick in average. It extends to 8 km from the coastline and has a minimum width of  $\sim 1.6$  km in its distal part. The thickness of the slide unit b is  $\sim 10$  m and approximately 20 m of sediments cover it.

### 4.2.2. Additional Deposits Around Offshore Seamounts

[27] Deposits have been identified around the Kahouanne Volcanoes. Deposit 10, located east of seamount B, extends for  $\sim 5$  km in a north-northeast direction with a width of 13 km, and covers an area of  $\sim 61$  km<sup>2</sup> (Figures 5d and 7). Its thickness ranges between  $\sim 135$  m (near the seamount) to 85 m, before thinning northeastward, giving an average thickness of  $\sim 111$  m and a volume of 4.3 km<sup>3</sup>. Well-bedded sedimentary layers from  $\sim 135$  m to  $\sim 185$  m thick cover the deposit 10 (up to 220 m above the deposit end; Figure 5d).

[28] South of seamount B a small chaotic unit (deposit 11; Figures 6 (line gwa33) and 7) is identified under deposit 8. A mean thickness of  $\sim 215$  m of sedimentary units separates the deposits. Deposit 11 covers an area of  $\sim 10$  km<sup>2</sup> and has a volume of  $\sim 0.4$  km<sup>3</sup>. West of seamount A, deposit 12 (Figures 6 (line gwa38) and 7) has dimensions of  $\sim 4.6$  km by  $\sim 1.2$  km ( $\sim 5.5$  km<sup>2</sup>), an average thickness of  $\sim 40$  m, and a volume of  $\sim 0.2$  km<sup>3</sup>.

## 5. Discussion

### 5.1. Morphological Characteristics of the Submarine Landslide Deposits

#### 5.1.1. Deposit Morphologies

[29] Ten large landslide deposits have now been identified offshore from Montserrat (deposit 1 to 12 excluding deposits 6 and 7 related to Redonda and Antigua islands; e.g., *Le Friant et al.* [2004]). The deposits can be divided into two types. The first type (deposits 1, 3 and 5) displays hummocky topography on the seafloor on swath bathymetry and seismic reflection profiles. The second type of deposit comprises shallowly buried (deposits 2, 4 and 12) or more deeply buried (deposits 8, 9, 10 and 11) units that display chaotic seismic signals beneath well-bedded reflectors. Hummock characteristics deduced from surficial deposits (Figure 3) show a range of forms, with symmetric or asymmetric,

sharp, rounded and flattened shapes. As is the case with subaerial deposits [Voight *et al.*, 2002], hummocky morphology leads to irregularities in the thickness of deposits along seismic profiles (Figures 4c and 6). These irregularities decrease away from the island as the number and the size of blocks decrease.

### 5.1.2. Lateral Margins of the Deposits

[30] On some profiles, sharp transitions between sedimentary and landslide-related units have been observed (Figure 6, line gwa44–40). Similar features were recognized by Deplus *et al.* [2001] for landslide deposits within the Grenada Basin in the southern part of the Lesser Antilles Arc but they also exist in other geological settings such as the big sedimentary landslides on the Norwegian continental margin, e.g., Storegga Slide [Bull *et al.*, 2009]. Deplus *et al.* [2001] and Le Friant *et al.* [2003a] interpreted these sharp margins as the result of erosional processes occurring during debris avalanche emplacement. On most profiles, a predominance of progressive transitions between sedimentary units and deposits have been underlined (e.g., decrease of ~30 m in 2.5 km for the thickness of deposit 2 on line gwa35-a; Figures 4c, 5b, 5d, and 6). The thinner deposit at the front of the chaotic unit probably results from the spreading of the debris avalanches [Le Friant *et al.*, 2003a].

### 5.1.3. Strong Reflectors

[31] The new high-resolution seismic data highlight the presence of strong reflectors hitherto unidentified within or at the base of several chaotic units (Figures 4b, 5a, 5b, 5c, and 6). Strong reflectors (generally flat and continuous) are clearly identified at the base of deposits 2 and 8. They represent a strong contrast in seismic impedance, likely the result of a lithological change between disturbed sediments immediately beneath the deposit and the chaotic unit above. We propose that these strong reflectors represent the basal shear surface of debris avalanches, as suggested by Bull *et al.* [2009] for the Storegga Slide deposit (Norwegian continental margin). Strong reflectors located within the central parts of slide deposits most likely separate different chaotic subunits, since they are generally discontinuous and irregular (Figure 6, line gwa38).

[32] It is of interest that comparable basal strong reflectors are seen within both deposits 2 and 8, and that the extent of these deposits is also similar. This suggests that similar overall flow, channelization

and emplacement processes influenced both deposits, and that such events may repeat through time with a similar pattern. This emplacement process pattern is potentially controlled by submarine bathymetry, as strongly influenced by local tectonics, such as in this case by the Bouillante-Montserrat half-graben fault system (see section 5.4).

## 5.2. Chronology of the Deposits

[33] Here, we briefly describe the successive emplacement of the deposits identified offshore Montserrat and around the Kahouanne Volcanoes. We propose a relative chronology based on the deposit depth and on overlying sediment thicknesses. The relationships with major fault systems (such as the BMFS, MHFS, BMAF) are also discussed.

[34] Sedimentation rates from previous studies of the Lesser Antilles volcanic arc have been used to estimate the age of landslide deposits around Montserrat. Le Friant *et al.* [2008] proposed a sedimentation rate about 2.3 cm kyr<sup>-1</sup> deduced from micropaleontology and stable isotope stratigraphy ( $\delta^{18}\text{O}$ ) studies on the CAR-MON 2 sediment core, which covers a period of ~250 kyr (length: 575 cm). However, this core was located ~55 km southwest of Montserrat (Figure 1). The rate they derived was thus unlikely to be representative of sedimentation occurring south of the island and within the Bouillante-Montserrat half-graben, given the volcanic activity and thick accumulations of pyroclastic deposits, turbidites and detrital sediments in this area. A maximum sedimentation rate of 29 cm kyr<sup>-1</sup> has been estimated from sediment core analysis in the southern part of the Lesser Antilles Arc (within the Grenada Basin [Boudon *et al.*, 2008]). The smaller scale of volcanic centers on Montserrat suggests that the maximum sedimentation rate off Montserrat is likely to be lower than that in the Grenada Basin. We therefore propose to use a nominal intermediate sedimentation rate of 15 cm kyr<sup>-1</sup> to characterize the offshore area south of Montserrat. Although we acknowledge that there are significant uncertainties involved in applying a single sedimentation rate across this area, this exercise provides an initial indication of the relative ages of different landslide deposits offshore Montserrat.

[35] The hummocky deposits 1, 3 and 5 were emplaced last and relative recently, given the absence of drape over the hyperbolic facies on the 3.5 kHz profiles that represent the deposit. An age of ~2 kyr was proposed for deposit 1 by Boudon *et al.* [2007] on the basis of <sup>14</sup>C dates obtained on noncarbonized

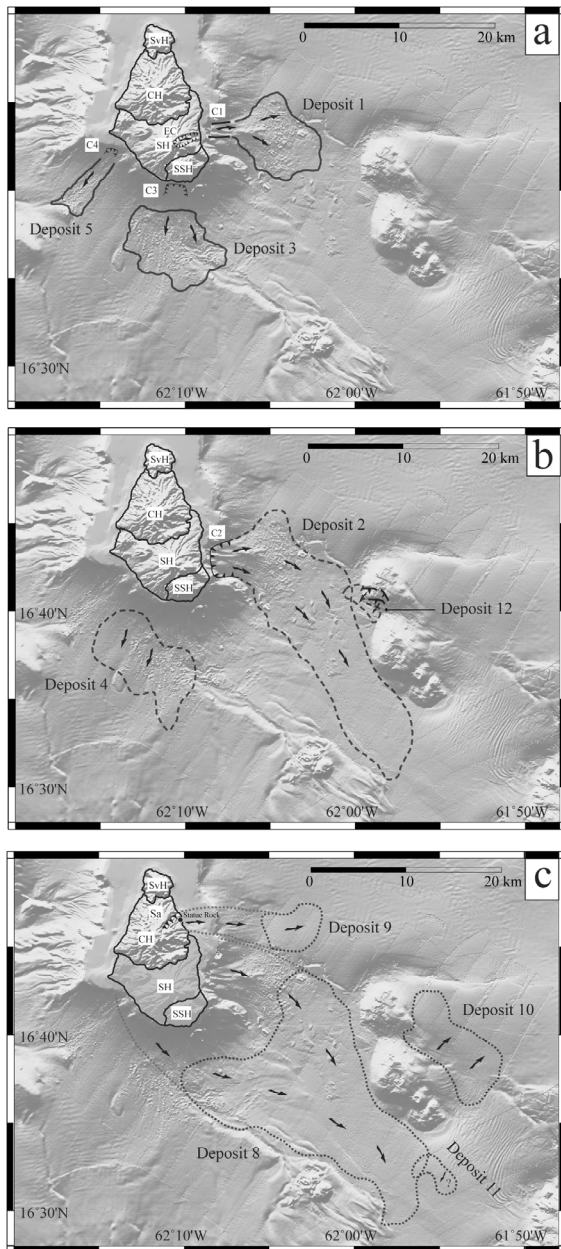


**Figure 8.** Maps showing the spatial relationships between the (a) surficial, (b) shallowly buried, and (c) deeply buried debris avalanche deposits, submarine troughs (C1, C2, C3, and C4), on-land flank collapse structures (Sa, structure a; EC, English's Crater) and on-land deposit (e.g., gray dot, Statue Rock).

wood samples in an island deposit provisionally correlated with this unit. Deposits 3 and 5 are probably very recent but their age cannot be constrained due to the lack of sedimentary drape. Deposit 2 is separated from deposit 1 by ~35 m of sediments, suggesting an age of emplacement at ~233 kyr. Regarding to the thickness of the sedi-

mentary units separating the deposit 2 to the deposit 8 (~100 m in average), deposit 2 appears to be ~665 kyr younger than deposit 8, giving an approximated age of 900 kyr for deposit 8. Deposit 11 is likely to be the oldest deposit identified within the Bouillante-Montserrat half-graben because of the thickness of overlying sediments. It is separated from deposit 8 by sedimentary units with a mean thickness of ~215 m, suggesting that a time period of ~1.5 Myr occurred between these two events.

### 5.3. Origin of the Landslide Deposits

[36] The landslide deposits identified offshore Montserrat are either related to subaerial flank collapses or failures of the surrounding submarine slopes (volcanic and/or sedimentary material).

#### 5.3.1. Submarine Surficial Deposits (1, 3, and 5)

[37] Deposit 1 is directly associated with the horse-shoe-shaped English's Crater, as shown by the continuity between the rims of the crater and the submarine embayment C1 (as documented by *Le Friant et al.* [2004]) (Figure 8a). The new seismic data (GWADASEIS, JC45/46) result in an increased volume estimate for deposit 1 of 1.8 km<sup>3</sup>. The dense-rock equivalent volume is about 1.35 km<sup>3</sup> which suggests that the English's Crater collapse event alone (0.5 km<sup>3</sup> [*Le Friant et al.*, 2004]) cannot account for deposit 1. The additional volume observed in deposit 1 could result from either (1) successive flank collapses (that may include a debris avalanche deposit identified in the coastal cliff and dated at 20 kyr [*Boudon et al.*, 2007]), rather than the previously suggested single event [*Le Friant et al.*, 2004] that formed English's Crater, (2) underwater slope failures concomitant with the English's Crater debris avalanche, and/or (3) eroded seafloor sediments incorporated within the mass flow during emplacement [*Le Friant et al.*, 2009]. The latter mechanism is common with gravitational mass flows and is referred to as bulking.

[38] Deposit 3 occurs adjacent to submarine embayment C3 (Figure 8a), and this association suggests that deposit 3 originated through a submarine slope failure [*Le Friant et al.*, 2004]. However, deposit 3 has a similar morphology to deposit 1 (see section 4), which has a subaerial collapse component. Deposit 3 may therefore also include failure of the subaerial as well as the submarine volcanic flanks, although any subaerial scar is now concealed by subsequent volcanic activity. Deposit 5 probably originates from a submarine

slope failure linked to embayment C4 [*Le Friant et al.*, 2004] (Figure 8a).

### 5.3.2. Shallowly Buried Deposits (2, 4, and 12)

[39] The high resolution of the new seismic reflection data shows more closely the link between deposit 2 and submarine embayment C2, suggesting that deposit 2 indeed resulted from failure of the submarine island flank [*Le Friant et al.*, 2004] (Figure 8b). The size and the extent (~30 km) of deposit 2 would suggest evolution of an initial debris avalanche into a debris flow. The strong reflectors at the base of deposit 2 are interpreted as being due to basal shear. The strong internal reflectors within deposit 2 may indicate two stages of emplacement.

[40] The new seismic data analysis modified the extent of deposit 4 and results in an increased estimate of its volume (~3.4 km<sup>3</sup>). The absence of clear structures on land or on the submarine slope prevents us from determining its origin. Thus, deposit 4 could either (1) result from an on-land flank collapse that affected both the old flank of the South Soufrière Hills-Soufrière Hills volcanic complex and its submarine part, later buried by subsequent volcanic activity, or (2) originate from a submarine slope failure. The thinning toward the southwest on the GWADASEIS seismic profiles (Figure 4c) indicates a southwesterly direction of deposit propagation (Figure 8b). A sediment core located above deposit 4 revealed the presence of a dark basaltic scoria deposit at its base [*Le Friant et al.*, 2004]. This deposit was related to the South Soufrière Hills Volcano, suggesting an age of, at least, 130 kyr [*Le Friant et al.*, 2004]. The location of deposit 4 below this deposit induces an age of >130 kyr. As proposed by *Le Friant et al.* [2004], deposit 4 could have been originated from an older flank collapse event, with the South Soufrière Hills Volcano infilling the collapse depression.

[41] The shape and the location of deposit 12, as well as the presence of associated flank scarps, suggest an origin in a flank failure of seamount A of the Kahouanne Volcanoes (Figure 8b).

### 5.3.3. Deeply Buried Deposits (8, 9, 10, and 11)

[42] The voluminous deposit 8 has been offset by faults of the MHFS and BMFS. Small offsets were identified between the lower limits of the two lobes on the seismic profiles (Figure 6, line gwa44–40). These offsets are interpreted as resulting from the deposition of syntectonic sediments [*Feuillet et al.*,

2010]. Using a maximum sedimentation rate of 15 cm kyr<sup>-1</sup> deposit 8 was emplaced ~900 kyr ago (section 5.2). At that time the active volcano of Montserrat was the Centre Hills Volcano (~950–550 kyr [*Harford et al.*, 2002]), and the South Soufrière Hills-Soufrière Hills volcano complex had not yet formed. Thus, an origin from the current submarine flanks of the South Soufrière Hills-Soufrière Hills volcanic complex (<170 kyr [*Harford et al.*, 2002]) is excluded. The deposit volume is ~20 km<sup>3</sup> and is of a similar order of magnitude to mass flow deposits recognized off Dominica, St Lucia and Martinique [*Deplus et al.*, 2001; *Le Friant et al.*, 2002; *Boudon et al.*, 2007]. The origin of deposit 8 (on-land flank collapse and/or submarine slope failure) cannot be determined due to subsequent volcanic activity of the island and/or erosion of related scarps. However, the volume and extent of deposit 8 would suggest more a submarine slope failure as origin, possibly in concomitance with a flank collapse event. The shape, as well as the magnitude of the deposit is of interest, given its unusual form of two lobes in the proximal region, merging into a single unit distally. The present-day form of the island suggests sources both east and south of Soufrière Hills, but it is clear from the dates of subaerial volcanic rocks that Soufrière Hills had not yet formed, and the sources areas of the lobes of deposit 8 are thus likely to be buried beneath younger volcanic rocks. However, the form of the deposit still requires an explanation, and it may be that the deposit, resulting from a failure off the Centre Hills Volcano, was forced around the proto-Soufrière Hills seamount, which may have been forming at this time (Figure 8c). In such a case, the early construction of the Soufrière Hills volcanic complex would have induced a deflection of the deposit, following the lowest bathymetric path, resulting in the formation of two lobes (Figure 6, line gwa44–40) which subsequently merged. However, deposit 8 can also have been formed before the construction of the proto-Soufrière Hills seamount and subsequently buried by its formation. Strong reflectors at the base of the deposit are likely to have a similar origin to those in deposit 2.

[43] Deposit 9 is located east of Centre Hills Volcano. A debris avalanche deposit identified on-land near the coastal cliff of Statue Rock on the northeast coast (Figure 8c), has been interpreted by *Boudon et al.* [2007] as the result of a subaerial flank collapse that affected the east flank of Centre Hills Volcano. It was associated to the scarp *Sa* described by *Le Friant et al.* [2004] (Figure 8c) and located on



**Figure 9.** Summary interpretation map showing the concentration of debris avalanche deposits toward the southeast surrounding quarter seafloor, within and around the Bouillante-Montserrat half-graben. The location of deposits shows an influence of the slopes of the Bouillante-Montserrat half-graben on their propagation, and repartition suggesting a major link between the formation of deposits offshore Montserrat and local fault systems (BMFS and BMAF). Inset: in dashed line, main extent of the chaotic deposits within the main fault systems (modified from *Feuillet et al.* [2010]) recognized offshore Montserrat.

the northwest bank of Bottomless Ghaut (Figure 1, inset). The continuity between the scarp *Sa* and the submarine deposit 9 suggests that both result from the same instability event on Centre Hills.

[44] The debris avalanche deposits 10 and 11, located near the Kahouanne Volcanoes, are probably related to one of the seamounts A or B. We propose that deposit 10 resulted from a flank collapse on the east side of the seamount B since it thins out roughly northeastward, suggesting a north-

northeast direction of propagation (Figure 8c). The scar located at the north of seamount B seems too insubstantial to be the source, but no other scar is visible.

#### 5.4. Distribution of the Deposits Resulting From Instabilities

[45] Mapping of the ten submarine deposits identified offshore Montserrat shows that most of the seafloor surrounding the island to the southeast

quarter is covered by debris avalanche and related debris flow deposits ( $\sim 520 \text{ km}^2$ ; Figure 9). Submarine landslide deposits are absent elsewhere (Figure 4a) as documented by the extensive grid of AGUADOMAR and CARAVAL seismic profiles located to the north and west of the island (Figure 2). Most of the debris avalanche deposits to the southeast of Montserrat (deposits 1, 2, 8, 11 and 12) are located within the Bouillante-Montserrat half-graben underlining a strong influence of the half-graben slopes on bathymetry, and hence on the distribution and propagation of deposits (Figures 7, 8, and 9). The other landslide deposits (deposits 3, 4, 5, 9 and 10) are not directly located within the half-graben but their sources are probably associated with the major fault systems bordering it (BMFS, BMAF). This concentration of deposits within and around the half-graben suggests a major link between the formation of debris avalanche and other mass flow deposits offshore Montserrat and local fault systems.

## 6. Conclusion

[46] This study again increases the number, frequency and total volume of submarine landslide deposits recognized around volcanic islands in the Lesser Antilles Arc [e.g., Boudon *et al.*, 2007] to 52 examples. Montserrat is now the first recognized island in the northern part of the Lesser Antilles Arc to have some submarine debris avalanche deposits with volumes up to  $\sim 10$  to  $20 \text{ km}^3$ . Such large volume deposits were previously observed only for volcanic islands further south in the arc (Martinique, St Lucia, Dominica). The large-scale structure of the islands (very steep slopes on the west contrasting with gentle slopes in the east) and the presence of the Grenada Basin controlled the occurrence of mass-wasting events in the southern part of the arc [e.g., Deplus *et al.*, 2001; Boudon *et al.*, 2007]. In this study, we find that most of the landslides off Montserrat are concentrated near major fault systems around and within the Bouillante-Montserrat half-graben suggesting, that the half-graben may play a similar role to the Grenada Basin further south in controlling the location of instabilities that result in mass-wasting events. Relatively small volcanic islands such as Montserrat can therefore be affected by repeated large-volume mass-wasting processes that deposit very large amounts of sediments into the surrounding basins. The ten landslide deposits recognized around Montserrat transported  $\sim 40 \text{ km}^3$  of material, which is equivalent to four times the annual

sediment supply from all of the world's present-day rivers [Talling *et al.*, 2007].

## Acknowledgments

[47] We thank the captains, officers, crews, and scientific teams of the N/O *L'Atalante*, N/O *Le Suroît* and RRS *James Cook*. We thank Yujin Choi for helpful technical support and Frédérique Leclerc for exchanges in Paris regarding the data. We acknowledge the MVO staff for logistic aspects during the marine surveys. We thank Barry Voight, Claudia Romagnoli, and Geoff Wadge for their fruitful reviews, which improved the paper. We used the GMT software developed by P. Wessel and W. Smith (available at <http://www.soest.hawaii.edu/gmt/>) for Figures 1, 2, 3, 7, and 8. IGP contribution 3151.

## References

- Boudon, G., A. Le Friant, J.-C. Komorowski, C. Deplus, and M. P. Semet (2007), Volcano flank instability in the Lesser Antilles Arc: Diversity of scale, processes, and temporal recurrence, *J. Geophys. Res.*, *112*, B08205, doi:10.1029/2006JB004674.
- Boudon, G., M. Paterne, J. Machault, B. Villemant, J.-C. Komorowski, and A. Le Friant (2008), Volcanic activity in the Lesser Antilles Arc: Correlation between on-land and marine tephrochronologic data, paper presented at 2008 General Assembly Volcanism, Int. Assoc. of Volcanol. and Chem. of the Earth's Inter., Reykjavik, Iceland, 17–22 Aug. 2008.
- Bouysse, P., D. Westercamp, and P. Andreieff (1990), The Lesser Antilles Island Arc, *Proc. Ocean Drill. Program Sci. Results*, *110*, 29–44.
- Bull, S., J. Cartwright, and M. Huuse (2009), A review of kinematic indicators from mass-transport complexes using 3D seismic data, *Mar. Pet. Geol.*, *26*, 1132–1151, doi:10.1016/j.marpetgeo.2008.09.011.
- Camus, G., and P. M. Vincent (1983), Discussion of a new hypothesis for the Krakatau volcanic eruption in 1883, *J. Volcanol. Geotherm. Res.*, *19*, 167–173, doi:10.1016/0377-0273(83)90130-0.
- Carracedo, J. C. (1999), Growth, structure, instability and collapse of Canarian volcanoes and comparisons with Hawaiian volcanoes, *J. Volcanol. Geotherm. Res.*, *94*, 1–19, doi:10.1016/S0377-0273(99)00095-5.
- Carracedo, J. C., S. J. Day, H. Guillou, and F. J. Pérez Torrado (1999), Giant Quaternary landslides in the evolution of La Palma and El Hierro, Canary Islands, *J. Volcanol. Geotherm. Res.*, *94*, 169–190, doi:10.1016/S0377-0273(99)00102-X.
- Clément, J. P., C. Legendre, M. Caroff, H. Guillou, J. Cotten, C. Bollinger, and G. Guille (2003), Epiclastic deposits and 'horseshoe-shaped' calderas in Tahiti (Society Islands) and Ua Huka (Marquesas Archipelago), French Polynesia, *J. Volcanol. Geotherm. Res.*, *120*, 87–101, doi:10.1016/S0377-0273(02)00366-9.
- Cohen, J. K., and J. J. W. Stockwell (1996), *CWP/SU: Seismic Unix Release 28: A Free Package for Seismic Research and Processing*, Colo. Sch. of Mines, Golden, Colo.
- Cole, P. D., E. S. Calder, R. S. J. Sparks, A. B. Clarke, T. H. Druitt, S. R. Young, R. A. Herd, C. L. Hardford, and G. E.

- Norton (2002), Deposits from dome collapse and fountain-collapse pyroclastic flows at Soufrière Hills Volcano, in *The Eruption of Soufrière Hills Volcano, Montserrat from 1995 to 1999*, edited by T. H. Druitt and B. P. Kokelaar, *Geol. Soc. London Mem.*, *21*, 231–262.
- Collot, J. Y., K. Lewis, G. Lamarche, and S. Lallemand (2001), The giant Ruatoria debris avalanche on the Northern Hikurangi Margin, New Zealand: Result of oblique seamount subduction, *J. Geophys. Res.*, *106*(B9), 19,271–19,297, doi:10.1029/2001JB900004.
- DeMets, C., P. E. Jansma, G. S. Mattioli, T. H. Dixon, F. Farina, R. Bilham, E. Calais, and P. Mann (2000), GPS geodetic constraints on Caribbean-North America plate motion, *Geophys. Res. Lett.*, *27*, 437–440, doi:10.1029/1999GL005436.
- Deplus, C., A. Le Friant, G. Boudon, J.-C. Komorowski, B. Villemant, C. Harford, J. Ségoufin, and J. L. Cheminée (2001), Submarine evidence for large-scale debris avalanches in the Lesser Antilles Arc, *Earth Planet. Sci. Lett.*, *192*, 145–157, doi:10.1016/S0012-821X(01)00444-7.
- Dufresne, A., S. Salinas, and C. Siebe (2010), Substrate deformation associated with the Jocotitlán edifice collapse and debris avalanche deposit, Central México, *J. Volcanol. Geotherm. Res.*, *197*, 133–148, doi:10.1016/j.jvolgeores.2010.02.019.
- Feuillet, N., et al. (2010), Active faulting induced by slip partitioning in Montserrat and link with volcanic activity: New Insights from the 2009 GWADASEIS marine cruise data, *Geophys. Res. Lett.*, *37*, L00E15, doi:10.1029/2010GL042556.
- Gee, M. J. R., R. L. Gawthorpe, and J. S. Friedmann (2005), Giant striations at the base of a submarine landslide, *Mar. Geol.*, *214*, 287–294, doi:10.1016/j.margeo.2004.09.003.
- Harford, C. L., M. S. Pringle, R. S. J. Sparks, and S. R. Young (2002), The volcanic evolution of Montserrat using <sup>40</sup>Ar/<sup>39</sup>Ar geochronology, in *The Eruption of Soufrière Hills Volcano, Montserrat from 1995 to 1999*, edited by T. H. Druitt and B. P. Kokelaar, *Geol. Soc. London Mem.*, *21*, 231–262.
- Hart, K., S. Carey, H. Sigurdsson, R. S. J. Sparks, and R. E. A. Robertson (2004), Discharge of pyroclastic flows into the sea during the 1996–1998 eruptions of the Soufrière Hills volcano, Montserrat, *Bull. Volcanol.*, *66*, 599–614, doi:10.1007/s00445-004-0342-1.
- Herd, R. A., M. Edmonds, and V. A. Bass (2005), Catastrophic lava dome failure at Soufrière Hills Volcano, Montserrat, 12–13 July 2003, *J. Volcanol. Geotherm. Res.*, *148*, 234–252, doi:10.1016/j.jvolgeores.2005.05.003.
- Kenedi, C. L., R. S. J. Sparks, P. Malin, B. Voight, S. Dean, T. Minshull, M. Paulatto, C. Pierce, and E. Shalev (2010), Contrasts in morphology and deformation offshore Montserrat: New insights from the SEA-CALIPSO marine cruise data, *Geophys. Res. Lett.*, *37*, L00E25, doi:10.1029/2010GL043925.
- Labazuy, P. (1996), Recurrent landslides events on the submarine flank of Piton de la Fournaise volcano (Reunion Island), in *Volcano Instability on the Earth and Other Planets*, edited by W. J. McGuire, A. P. Jones, and J. Neuberg, *Geol. Soc. Spec. Publ.*, *110*, 295–306.
- Le Friant, A., G. Boudon, J.-C. Komorowski, and C. Deplus (2002), L'île de la Dominique, à l'origine des avalanches de débris les plus volumineuses de l'arc des Petites Antilles, *C. R. Geosci.*, *334*, 235–243, doi:10.1016/S1631-0713(02)01742-X.
- Le Friant, A., G. Boudon, C. Deplus, and B. Villemant (2003a), Large-scale flank collapse events during the activity of Montagne Pelée, Martinique, Lesser Antilles, *J. Geophys. Res.*, *108*(B1), 2055, doi:10.1029/2001JB001624.
- Le Friant, A., P. Heinrich, C. Deplus, and G. Boudon (2003b), Numerical simulation of the last flank-collapse event of Montagne Pelée, Martinique, Lesser Antilles, *Geophys. Res. Lett.*, *30*(2), 1034, doi:10.1029/2002GL015903.
- Le Friant, A., C. L. Harford, C. Deplus, G. Boudon, R. S. J. Sparks, R. A. Herd, and J.-C. Komorowski (2004), Geomorphological evolution of Montserrat (West Indies): Importance of flank collapse and erosional processes, *J. Geol. Soc.*, *161*, 147–160, doi:10.1144/0016-764903-017.
- Le Friant, A., G. Boudon, J.-C. Komorowski, P. Heinrich, and M. P. Semet (2006), Potential flank-collapse of Soufrière volcano, Guadeloupe, Lesser Antilles? Numerical simulation and hazards, *Nat. Hazards*, *39*, 381–393, doi:10.1007/s11069-005-6128-8.
- Le Friant, A., E. J. Lock, M. B. Hart, G. Boudon, R. S. J. Sparks, M. J. Leng, C. W. Smart, J.-C. Komorowski, C. Deplus, and J. K. Fisher (2008), Late Pleistocene tephrochronology of marine sediments adjacent to Montserrat, Lesser Antilles volcanic arc, *J. Geol. Soc.*, *165*, 279–289, doi:10.1144/0016-76492007-019.
- Le Friant, A., C. Deplus, G. Boudon, R. S. J. Sparks, J. Trofimovs, and P. Talling (2009), Submarine deposition of volcanoclastic material from the 1995–2005 eruptions of Soufrière Hills volcano, Montserrat, *J. Geol. Soc.*, *166*, 171–182, doi:10.1144/0016-76492008-047.
- Le Friant, A., et al. (2010), Eruption of Soufrière Hills (1995–2009) from an offshore perspective: Insights from repeated swath bathymetry surveys, *Geophys. Res. Lett.*, *37*, L11307, doi:10.1029/2010GL043580.
- Martin-Kaye, P. H. A. (1969), A summary of the geology of the Lesser Antilles, *Overseas Geol. Miner. Resour.*, *10*(2), 172–206.
- Masson, D. G., A. B. Watts, M. J. R. Gee, R. Urgeles, N. C. Mitchell, T. P. Le Bas, and M. Canals (2002), Slope failures on the flanks of the western Canary Islands, *Earth Sci. Rev.*, *57*, 1–35, doi:10.1016/S0012-8252(01)00069-1.
- McGuire, W. J. (1996), Volcano instability: A review of contemporary themes, in *Volcano Instability on the Earth and Other Planets*, edited by W. J. McGuire, A. P. Jones, and J. Neuberg, *Geol. Soc. Spec. Publ.*, *110*, 1–23.
- Moore, J. G., D. A. Clague, R. T. Holcomb, P. W. Lipman, W. R. Normark, and M. E. Torresan (1989), Prodigious submarine landslides on the Hawaiian ridge, *J. Geophys. Res.*, *94*, 17,465–17,484, doi:10.1029/JB094iB12p17465.
- Oehler, J. F., P. Labazuy, and J. F. Lénat (2004), Recurrence of major flank landslides during the last 2-Ma-history of Reunion Island, *Bull. Volcanol.*, *66*, 585–598, doi:10.1007/s00445-004-0341-2.
- Oehler, J. F., J. F. Lénat, and P. Labazuy (2008), Growth and collapse of La Reunion Island volcanoes, *Bull. Volcanol.*, *70*, 717–742, doi:10.1007/s00445-007-0163-0.
- Paulatto, M., et al. (2010), Upper crustal structure of an active volcano from refraction/reflection tomography, Montserrat, Lesser Antilles, *Geophys. J. Int.*, *180*, 685–696, doi:10.1111/j.1365-246X.2009.04445.x.
- Schneider, J. C., et al. (1997), Du volcan au sédiment: La dynamique du talus volcanoclastique sous-marin de Gran Canaria, Canaries (Atlantique orientale, Leg ODP 157), *C. R. Acad. Sci., Ser. IIa: Sci. Terre Planetes*, *324*, 891–898.
- Siebert, L. (1984), Large volcanic debris avalanches: Characteristics of source areas, deposits, and associated eruptions, *J. Volcanol. Geotherm. Res.*, *22*, 163–197, doi:10.1016/0377-0273(84)90002-7.

- Smith, W. H. F., and D. T. Sandwell (1997), Global sea floor topography from satellite altimetry and ship depth soundings, *Science*, 277, 1956–1962, doi:10.1126/science.277.5334.1956.
- Sparks, R. S. J., J. Barclay, E. S. Calder, R. A. Herd, J.-C. Komorowski, R. Luckett, G. E. Norton, L. J. Ritchie, B. Voight, and A. W. Woods (2002), Generation of a debris avalanche and violent pyroclastic density current on 26 December (Boxing Day) 1997 at Soufrière Hills Volcano, in *The Eruption of Soufrière Hills Volcano, Montserrat from 1995 to 1999*, edited by T. H. Druitt and B. P. Kokelaar, *Geol. Soc. London Mem.*, 21, 409–434.
- Talling, P. J., et al. (2007), Onset of submarine debris flow deposition far from original giant landslide, *Nature*, 450, 541–544, doi:10.1038/nature06313.
- Tinti, S., G. Pagnoni, and F. Zaniboni (2006), The landslides and tsunamis of the 30th of December 2002 in Stromboli analysed through numerical simulations, *Bull. Volcanol.*, 68(5), 462–479, doi:10.1007/s00445-005-0022-9.
- Trofimovs, J., et al. (2006), Submarine pyroclastic deposits formed at the Soufrière Hills volcano, Montserrat (1995–2003), What happens when pyroclastic flows enter the ocean?, *Geology*, 34(7), 549–552, doi:10.1130/G22424.1.
- Trofimovs, J., R. S. J. Sparks, and P. J. Talling (2008), Anatomy of a submarine pyroclastic flow and associated turbidity current: July 2003 dome collapse event, Soufrière Hills volcano, Montserrat, West Indies, *Sedimentology*, 55, 617–634, doi:10.1111/j.1365-3091.2007.00914.x.
- Ui, T., S. Takarada, and M. Yoshimoto (2000), Debris avalanches, in *Encyclopedia of Volcanoes*, edited by H. Sigurdsson and B. F. Houghton, pp. 617–626, Academic, San Diego, Calif.
- Urgeles, R., M. Canals, J. Baraza, B. Alonso, and D. Masson (1997), The most recent megalandslides of the Canary Islands: El Golfo debris avalanche and Canary debris flow, west El Hierro Island, *J. Geophys. Res.*, 102(B9), 20,305–20,323, doi:10.1029/97JB00649.
- Voight, B. (2000), Stability of andesite volcanoes and lava domes, *Philos. Trans. R. Soc. A*, 358, 1663–1703, doi:10.1098/rsta.2000.0609.
- Voight, B., and D. Elsworth (1997), Failure of volcano slopes, *Geotechnique*, 47, 1–31, doi:10.1680/geot.1997.47.1.1.
- Voight, B., et al. (2002), The 26 December (Boxing Day) 1997 sector collapse and debris avalanche at Soufrière Hills Volcano, in *The Eruption of Soufrière Hills Volcano, Montserrat from 1995 to 1999*, edited by T. H. Druitt and B. P. Kokelaar, *Geol. Soc. London Mem.*, 21, 363–407.
- Wadge, G. (1984), Comparison of volcanic production rates and subduction rates in the Lesser Antilles and Central America, *Geology*, 12, 555–558, doi:10.1130/0091-7613(1984)12<555:COVPR>2.0.CO;2.
- Wadge, G., R. Herd, G. Ryan, E. S. Calder, and J.-C. Komorowski (2010), Lava production at Soufrière Hills Volcano, Montserrat: 1995–2009, *Geophys. Res. Lett.*, 37, L00E03, doi:10.1029/2009GL041466.